

Institute for Aerospace Studies
UNIVERSITY OF TORONTO
Centre for Research in Sustainable Aviation

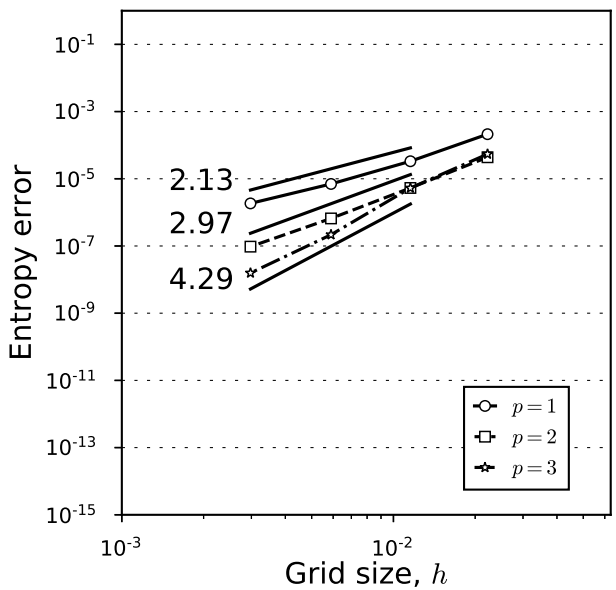
Development and Investigation of Accurate High-Order Generalized Summation-by-Parts Discretizations for Computational Fluid Dynamics

David A. Craig Penner and David W. Zingg
University of Toronto Institute for Aerospace Studies

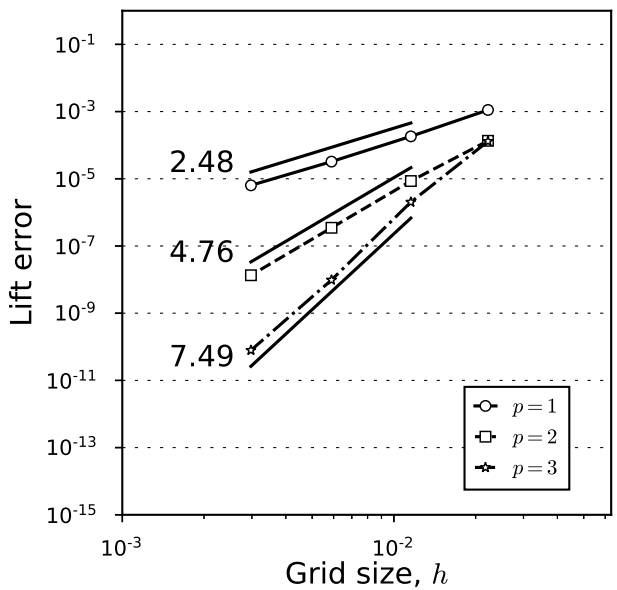
Advanced Modelling & Simulation (AMS) Seminar Series
NASA Ames Research Center
March 3, 2022

Motivation

- **High-order methods**
  - potentially very efficient for many problems involving the numerical solution of turbulent fluid flows
- **Generalized summation-by-parts (SBP) methods**
  - high-order, provably conservative, provably linearly and nonlinearly stable, amenable to complex geometries and parallelization
- **Superconvergent functionals**
  - very attractive in the context of, for example, aerodynamic shape optimization



Solution error



Functional error

Objectives

Overarching goal:

- Investigate and improve high-order tensor-product discretizations based on the generalized SBP property with a specific focus on delineating the requirements for obtaining accurate solutions and functionals.

Main objectives:

1. Develop components of high-order flow solvers including novel artificial dissipation operators and approaches for high-order grid generation and refinement.

2. Show that functional superconvergence is retained for generalized SBP discretizations of sufficiently smooth problems governed by the linear convection equation in curvilinear coordinates.

3. Develop generalized SBP methods for obtaining superconvergent functionals when solving sufficiently smooth problems governed by the Euler equations. Delineate the key features of a discretization having an impact on solution and functional accuracy including the representation of the geometry, the approximation of the metrics, and the approximation of the wall normal in the flow tangency boundary condition.

Definition of 1D SBP operator

Definition of 1D SBP operator for the first derivative*:

A matrix operator, $\mathsf{D}_{\xi_l}^{(1\mathrm{D})} \in \mathbb{R}^{N_l \times N_l}$, is an SBP operator that approximates the derivative $\frac{\partial}{\partial \xi_l}$, on the domain $\xi_l \in [\alpha_{\xi_l}, \beta_{\xi_l}]$ discretized with N_l nodes, of degree p if

1. $\mathsf{D}_{\xi_l}^{(1\mathrm{D})} \boldsymbol{\xi}_l^k = \left(\mathsf{H}_{\xi_l}^{(1\mathrm{D})}\right)^{-1} \mathsf{Q}_{\xi_l}^{(1\mathrm{D})} \boldsymbol{\xi}_l^{k-1} = k \boldsymbol{\xi}_l^{k-1}, \quad k = 0, 1, \ldots, p;$
2. $\mathsf{H}_{\xi_l}^{(1\mathrm{D})}$, the norm matrix, is symmetric and positive definite; and
3. $\mathsf{Q}_{\xi_l}^{(1\mathrm{D})} + \left(\mathsf{Q}_{\xi_l}^{(1\mathrm{D})}\right)^{\mathrm{T}} = \mathsf{E}_{\xi_l}^{(1\mathrm{D})}$, where $\left(\boldsymbol{\xi}_l^i\right)^{\mathrm{T}} \mathsf{E}_{\xi_l}^{(1\mathrm{D})} \boldsymbol{\xi}_l^j = \beta_{\xi_l}^{i+j} - \alpha_{\xi_l}^{i+j}, \quad i, j, = 0, 1, \ldots r, r \geq p.$

Decomposition of $\mathsf{E}_{\xi_l}^{(1\mathrm{D})}$:

$$\mathsf{E}_{\xi_l}^{(1\mathrm{D})} = \boldsymbol{t}_{\beta_{\xi_l}} \boldsymbol{t}_{\beta_{\xi_l}}^{\mathrm{T}} - \boldsymbol{t}_{\alpha_{\xi_l}} \boldsymbol{t}_{\alpha_{\xi_l}}^{\mathrm{T}}, \text{ where } \boldsymbol{t}_{\alpha_{\xi_l}}^{\mathrm{T}} \boldsymbol{\xi}_l^k = \alpha_{\xi_l}^k, \; \boldsymbol{t}_{\beta_{\xi_l}}^{\mathrm{T}} \boldsymbol{\xi}_l^k = \beta_{\xi_l}^k, \; k = 0, 1, \ldots, r$$

where $\boldsymbol{t}_{\beta_{\xi_l}}$ and $\boldsymbol{t}_{\alpha_{\xi_l}}$ are extrapolation operators

Multidimensional operators:

- in the present work, multidimensional operators constructed on structured grids via Kronecker tensor-product formalism
- truly multidimensional SBP operators on unstructured grids have been derived (e.g., Hicken *et al.* [SISC 2016])

*Del Rey Fernández *et al.* [JCP 2014]

Summation-by-parts property

SBP property:

- describes the relationship between integration-by-parts and summation-by-parts

$$\underbrace{\int_{\hat{\Omega}_\kappa} \mathcal{P}_\kappa \frac{\partial \mathcal{Q}_\kappa}{\partial \xi_l}\, d\hat{\Omega}}_{\wr\!\wr} + \underbrace{\int_{\hat{\Omega}_\kappa} \frac{\partial \mathcal{P}_\kappa}{\partial \xi_l} \mathcal{Q}_\kappa\, d\hat{\Omega}}_{\wr\!\wr} = \underbrace{\oint_{\hat{\Gamma}_\kappa} \mathcal{P}_\kappa \mathcal{Q}_\kappa n_{\xi_l}\, d\hat{\Gamma}}_{\wr\!\wr}$$

$$\overbrace{\boldsymbol{p}_\kappa^{\mathrm{T}} \mathsf{H} \mathsf{D}_{\xi_l} \boldsymbol{q}_\kappa} + \overbrace{\boldsymbol{p}_\kappa^{\mathrm{T}} (\mathsf{H} \mathsf{D}_{\xi_l})^{\mathrm{T}} \boldsymbol{q}_\kappa} = \overbrace{\boldsymbol{p}_\kappa^{\mathrm{T}} \mathsf{E}_{\xi_l} \boldsymbol{q}_\kappa}$$

Uses include:

- proving conservation, proving stability, proving dual consistency, etc.

Some SBP operators that can be applied as traditional operators

- Classical SBP operators
  Kreiss & Scherer [Math. 1974]
  - uniform nodal distribution
  - include boundary nodes
  - repeated interior operator

$$\mathsf{D}_{\xi_1}^{(1\mathrm{D})} = \begin{bmatrix} -1 & 1 & & & \\ -\frac{1}{2} & 0 & \frac{1}{2} & & \\ & \ddots & \ddots & \ddots & \\ & & -\frac{1}{2} & 0 & \frac{1}{2} \\ & & & -1 & 1 \end{bmatrix}$$

- Hybrid Gauss-trapezoidal-Lobatto (HGTL) and hybrid Gauss-trapezoidal (HGT)*
  - uniform interior nodal distribution, nonuniform near boundaries
  - HGTL includes boundary nodes, HGT does not
  - repeated interior operator

- Optimal SBP operators of Mattsson *et al.* [JCP 2014, JCP 2018]
  - uniform interior nodal distribution, nonuniform near boundaries
  - include boundary nodes
  - repeated interior operator
  - first two truncation error terms are minimized:

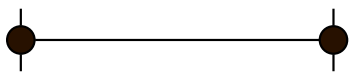
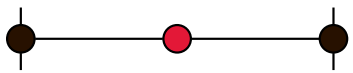
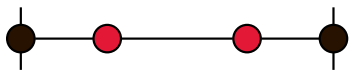
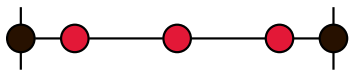
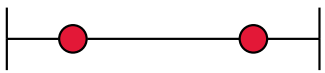
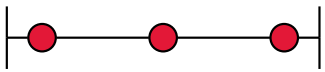
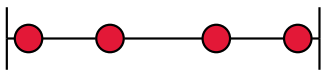
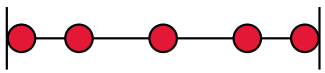
$$\|\mathbf{err}_{p+1}\|_{\mathsf{H}}^2 + \|\mathbf{err}_{p+2}\|_{\mathsf{H}}^2$$

*Del Rey Fernández & Zingg [SISC 2015]

Some purely element-type SBP operators*

LGL → Legendre-Gauss-Lobatto

LG → Legendre-Gauss

	Nodal distribution	*Operator degree,* p	*Extrapolation degree,* r	*Quadrature degree,* τ
LGLp1		1	∞	$2p-1=1$
LGLp2		2	∞	$2p-1=3$
LGLp3		3	∞	$2p-1=5$
LGLp4		4	∞	$2p-1=7$
LGp1		1	1	$2p+1=3$
LGp2		2	2	$2p+1=5$
LGp3		3	3	$2p+1=7$
LGp4		4	4	$2p+1=9$

*see Carpenter & Gottlieb [JCP 1996] and Del Rey Fernández *et al.* [JCP 2014]

Artificial dissipation

Motivation:

- use of the preceding operators with simultaneous approximation terms sufficient for linear problems, volume dissipation can be needed for nonlinear problems

Goal:

- outline different options for incorporating dissipation via two-element example, describe volume dissipation operators

1D linear convection equation:

$$\frac{\partial \mathcal{U}}{\partial t} + a \frac{\partial \mathcal{U}}{\partial x} = 0$$

- assume well-posed initial and boundary conditions

SBP-SAT discretization in left element (similar in right element):

$$\operatorname{diag}\left(\mathcal{J}_h\right)^{\mathrm{L}} \frac{d\boldsymbol{u}_h^{\mathrm{L}}}{dt} + a \mathsf{D}_{\xi_1}^{(1\mathrm{D})} \boldsymbol{u}_h^{\mathrm{L}} =$$
$$\underbrace{\sigma^{\mathrm{L}} \left(\mathsf{H}_{\xi_1}^{(1\mathrm{D})}\right)^{-1} \boldsymbol{t}_{\beta_{\xi_1}} \left(\boldsymbol{t}_{\beta_{\xi_1}}^{\mathrm{T}} \boldsymbol{u}_h^{\mathrm{L}} - \boldsymbol{t}_{\alpha_{\xi_1}}^{\mathrm{T}} \boldsymbol{u}_h^{\mathrm{R}}\right)}_{\text{interface SAT}} \underbrace{- |a| \left(\mathsf{H}_{\xi_1}^{(1\mathrm{D})}\right)^{-1} \mathsf{S}}_{\text{dissipation model}} \boldsymbol{u}_h^{\mathrm{L}}$$

Dissipation analysis via energy method

Apply the energy method:

- multiply by the solution and integrate in space to obtain

$$\frac{d}{dt}\left(\left\|\boldsymbol{u}_h^{\mathrm{L}}\right\|^2_{\mathsf{H}^{(1\mathrm{D})}_{\xi_1}\,\mathrm{diag}\left(\mathcal{J}_h\right)^{\mathrm{L}}}+\left\|\boldsymbol{u}_h^{\mathrm{R}}\right\|^2_{\mathsf{H}^{(1\mathrm{D})}_{\xi_1}\,\mathrm{diag}\left(\mathcal{J}_h\right)^{\mathrm{R}}}\right)$$

$$=\begin{bmatrix}\boldsymbol{t}^{\mathrm{T}}_{\beta_{\xi_1}}\boldsymbol{u}_h^{\mathrm{L}} & \boldsymbol{t}^{\mathrm{T}}_{\alpha_{\xi_1}}\boldsymbol{u}_h^{\mathrm{R}}\end{bmatrix}\begin{bmatrix}2\sigma^{\mathrm{L}}-a & -\left(\sigma^{\mathrm{L}}+\sigma^{\mathrm{R}}\right)\\ -\left(\sigma^{\mathrm{L}}+\sigma^{\mathrm{R}}\right) & 2\sigma^{\mathrm{R}}+a\end{bmatrix}\begin{bmatrix}\boldsymbol{t}^{\mathrm{T}}_{\beta_{\xi_1}}\boldsymbol{u}_h^{\mathrm{L}}\\ \boldsymbol{t}^{\mathrm{T}}_{\alpha_{\xi_1}}\boldsymbol{u}_h^{\mathrm{R}}\end{bmatrix}-2\left|a\right|\begin{bmatrix}\boldsymbol{u}_h^{\mathrm{L}} & \boldsymbol{u}_h^{\mathrm{R}}\end{bmatrix}\begin{bmatrix}\mathsf{S} & \\ & \mathsf{S}\end{bmatrix}\begin{bmatrix}\boldsymbol{u}_h^{\mathrm{L}}\\ \boldsymbol{u}_h^{\mathrm{R}}\end{bmatrix}$$

$$=\underbrace{\sigma\left|a\right|\begin{bmatrix}\boldsymbol{t}^{\mathrm{T}}_{\beta_{\xi_1}}\boldsymbol{u}_h^{\mathrm{L}} & \boldsymbol{t}^{\mathrm{T}}_{\alpha_{\xi_1}}\boldsymbol{u}_h^{\mathrm{R}}\end{bmatrix}\begin{bmatrix}-1 & 1\\ 1 & -1\end{bmatrix}\begin{bmatrix}\boldsymbol{t}^{\mathrm{T}}_{\beta_{\xi_1}}\boldsymbol{u}_h^{\mathrm{L}}\\ \boldsymbol{t}^{\mathrm{T}}_{\alpha_{\xi_1}}\boldsymbol{u}_h^{\mathrm{R}}\end{bmatrix}}_{\text{interface dissipation}}\underbrace{-2\left|a\right|\begin{bmatrix}\boldsymbol{u}_h^{\mathrm{L}} & \boldsymbol{u}_h^{\mathrm{R}}\end{bmatrix}\begin{bmatrix}\mathsf{S} & \\ & \mathsf{S}\end{bmatrix}\begin{bmatrix}\boldsymbol{u}_h^{\mathrm{L}}\\ \boldsymbol{u}_h^{\mathrm{R}}\end{bmatrix}}_{\text{volume dissipation}}.$$

- upwind SATs ($\sigma = 1$) $\rightarrow$ interface dissipation
- symmetric SATs ($\sigma = 0$) $\rightarrow$ no interface dissipation
- S = symmetric positive-definite $\rightarrow$ volume dissipation
- $\mathsf{S} = 0 \rightarrow$ no volume dissipation

Artificial dissipation operators

Volume dissipation model:

$$\boldsymbol{u}^{\mathrm{T}}\mathsf{H}\mathsf{A}_{\mathsf{D}}\boldsymbol{u} = -\varepsilon\Delta x_{\mathsf{avg}}^{2s-1}\left(\mathsf{M}\boldsymbol{u}\right)^{\mathrm{T}}\mathsf{C}\mathsf{M}\boldsymbol{u} \approx -\varepsilon\Delta x_{\mathsf{avg}}^{2s-1}\int_{x_{\mathrm{L}}}^{x_{\mathrm{R}}}|a|\left(\frac{\partial^{s}\mathcal{U}}{\partial x^{s}}\right)^{2}dx$$

- model approximates dissipative term
- $\varepsilon \in [0.001, 0.04] \rightarrow$ dissipation coefficient
- $s = p + 1 \rightarrow$ parameter related to the order of the dissipation
- $\mathsf{C} \rightarrow$ symmetric positive-definite matrix, e.g., $\mathsf{C} = \mathsf{H}\,|a|$

For classical SBP operators, matrix M given in:

- Mattsson *et al.* [JSC 2004], Diener *et al.* [JSC 2007]

For more general SBP operators (e.g., HGTL, HGT, Mattsson's optimal SBP operators), matrix M constructed by introducing unknowns near boundaries and solving linear system of equations

High-order grid generation

Procedure:

1. read in (x_1, x_2) coordinates of initial
2. set up mapping of prescribed polynomial degree on each element:
   $(x_1, x_2) = \mathcal{M}_\kappa(\xi_1, \xi_2) := \sum_{i,j=1}^{\overline{N}} \overline{\boldsymbol{x}}(\overline{\boldsymbol{\xi}}_{ij}) f_i(\xi_1) f_j(\xi_2)$
   - Lagrange interpolation approach*: use initial (x_1, x_2) nodes as interpolation points $\overline{\boldsymbol{x}}(\overline{\boldsymbol{\xi}}_{ij})$, use Lagrange polynomials $\ell_i(\xi_1), \ell_j(\xi_2)$ as basis functions $f_i(\xi_1), f_j(\xi_2)$

$$\ell_i(\xi_1) := \prod_{\substack{m=1 \\ m \neq i}}^{\overline{N}_1} \frac{\xi_1 - \overline{\xi}_{1,m}}{\overline{\xi}_{1,i} - \overline{\xi}_{1,m}}, \quad i = 1, \ldots, \overline{N}_1$$

   - B-spline approach**: fit initial grid in a least-squares sense to obtain suitable control points $\overline{\boldsymbol{x}}(\overline{\boldsymbol{\xi}}_{ij})$, use B-splines $\mathcal{N}_i^{(p_g+1)}(\xi_1), \mathcal{N}_j^{(p_g+1)}(\xi_2)$ as basis functions $f_i(\xi_1), f_j(\xi_2)$
3. update (ξ_1, ξ_2) nodes in reference space to correspond to nodes of the operator of interest
4. calculate (x_1, x_2) coordinates of new grid in physical space based on updated mapping and write new grid

---

*see Hindenlang [Phd thesis 2014]

**see Hicken & Zingg [AIAA 2010] and Del Rey Fernández *et al.* [JSC 2019]

1D model problem (primal)

Goal:

- introduce concept of dual consistency and examine superconvergence in 1D setting

Continuous: find $\mathcal{U}$ and evaluate output $\mathcal{I}(\mathcal{U})$

$$\text{PDE: } \frac{d\mathcal{U}(x)}{dx} = \mathcal{F}(x) \quad \text{in } \Omega \subset \mathbb{R}^d$$
$$\text{BC: } \quad \mathcal{U}(x=0) = \mathcal{U}_\text{L} \quad \text{on } \partial\Omega$$

Dual-weighted residual*:

$$\mathsf{R}(\mathcal{U}, \psi) := \int_\Omega \psi \left(\mathcal{F}(x) - \frac{d\mathcal{U}(x)}{dx} \right) dx - \psi(\mathcal{U} - \mathcal{U}_\text{L})|_{x=0}$$

Output functional:

$$\mathcal{I}(\mathcal{U}) := \int_\Omega \mathcal{G}\mathcal{U}\, dx + \alpha\mathcal{U}|_{x=1} + \underbrace{\mathsf{R}(\mathcal{U}, \psi)}_{=0}$$

Discrete (SBP): find $\boldsymbol{u}_h$ and evaluate output $\mathcal{I}_h(\boldsymbol{u}_h)$

$$\text{PDE + BC: } \mathsf{D}\boldsymbol{u}_h = \boldsymbol{f} - \mathsf{H}^{-1}\boldsymbol{t}_\text{L}(\boldsymbol{t}_\text{L}^\text{T}\boldsymbol{u}_h - \mathcal{U}_\text{L})$$

*see Becker & Rannacher [IWR 1996, Acta 2001] and Hicken [JCP 2012]

Corresponding dual problem and dual consistency

Equivalent functional representation:

$$\mathcal{I}(\psi) = \int_\Omega \psi \mathcal{F}\, dx + \psi \mathcal{U}_\mathrm{L}|_{x=0} + \underbrace{\mathsf{R}^*(\psi, \mathcal{U})}_{\text{dual residual}}$$

Dual residual:

$$\mathsf{R}^*(\psi, \mathcal{U}) := \int_\Omega \mathcal{U} \left(\mathcal{G}(x) + \frac{d\psi(x)}{dx} \right) dx - \mathcal{U}(\psi - \alpha)|_{x=1}$$

Continuous:

$$\begin{aligned} &\text{PDE:} \quad -\frac{d\psi(x)}{dx} = \mathcal{G}(x), \quad x \in \Omega \\ &\text{BC:} \quad \psi(x=1) = \alpha \end{aligned}$$

Discrete functional and dual residual:

$$\begin{aligned} \mathcal{I}_h(\boldsymbol{u}_h) &= \boldsymbol{g}^\mathrm{T} \mathsf{H} \boldsymbol{u}_h + \alpha \boldsymbol{t}_\mathrm{R}^\mathrm{T} \boldsymbol{u}_h + \mathsf{R}_h(\boldsymbol{\psi}_h, \boldsymbol{u}_h) \\ \mathsf{R}_h^*(\boldsymbol{\psi}_h, \boldsymbol{u}_h) &= \boldsymbol{u}_h^\mathrm{T} \mathsf{H}(\boldsymbol{g} + \mathsf{D}\boldsymbol{\psi}_h) - \boldsymbol{u}_h^\mathrm{T} \boldsymbol{t}_\mathrm{R}(\boldsymbol{t}_\mathrm{R}^\mathrm{T} \boldsymbol{\psi}_h - \alpha) \\ &= \boldsymbol{u}_h^\mathrm{T} \mathsf{H}(\underbrace{\boldsymbol{g} + \mathsf{D}\boldsymbol{\psi}_h - \mathsf{H}^{-1} \boldsymbol{t}_\mathrm{R}(\boldsymbol{t}_\mathrm{R}^\mathrm{T} \boldsymbol{\psi}_h - \alpha)}_{-\mathsf{D}\boldsymbol{\psi}_h = \boldsymbol{g} - \mathsf{H}^{-1} \boldsymbol{t}_\mathrm{R}(\boldsymbol{t}_\mathrm{R}^\mathrm{T} \boldsymbol{\psi}_h - \alpha)}) \end{aligned}$$

$\therefore$ discretization is dual consistent

Functional accuracy estimate—hyperbolic PDEs

Without a curvilinear transformation:[*]

$$|\mathcal{I}(\mathcal{U}) - \mathcal{I}_h(\boldsymbol{u}_h)| \lesssim \mathcal{O}(h^{\min(2p+1,\tau+1)})$$

$\tau \rightarrow$ degree of quadrature

With a curvilinear transformation, extrapolation operators of degree $r \geq 2p$ are required to preserve superconvergent functionals when:

- the Jacobian/ metrics of the transformation are approximated by the same SBP operator that is associated with the norm
- a higher degree representation of the geometry is used compared to the degree of the SBP operator used to discretize the flux terms

[*] Craig Penner & Zingg [JSC 2020], based on Hicken & Zingg [SISC 2011] and Boom [PhD thesis 2015]

1D boundary-value problem and grid functions

Purpose:

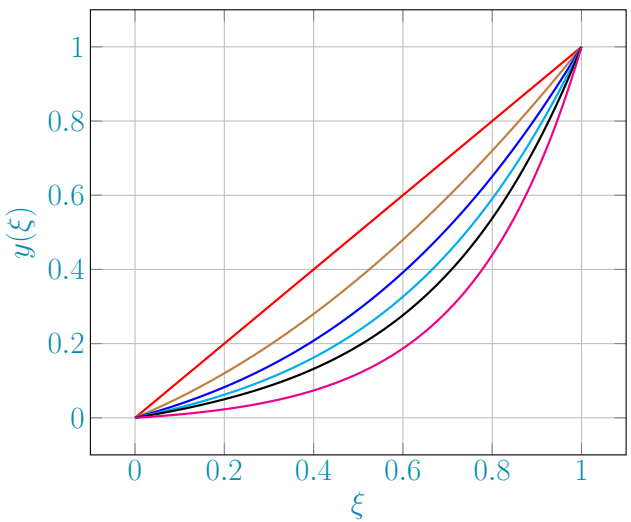
- verify functional accuracy estimate numerically

Source term and solution:

$$\mathcal{F}(x) = \frac{\pi e^x}{e-1}\cos\left(\frac{\pi e^x - \pi + e - 1}{e-1}\right) \quad \text{and} \quad \mathcal{U}(x) = \sin\left(\frac{\pi(e^x-1)}{e-1} + 1\right)$$

Continuous and discrete integral functionals:

$$\mathcal{I}(\mathcal{U}) = \int_0^1 \mathcal{U} dx = \int_0^1 \mathcal{U}\frac{dx}{d\xi}d\xi \quad \text{and} \quad \mathcal{I}_h(\boldsymbol{u}_h) = \sum_{i=1}^{n_e} \mathbf{1}^{\mathrm{T}}\mathsf{HJ}_i(\boldsymbol{u}_h)_i \approx \mathcal{I}(\mathcal{U})$$



Degree	*Grid Function,* $y(\xi)$
1	ξ
2	$\frac{1}{2}\xi^2 + \frac{1}{2}\xi$
3	$\frac{1}{3}\xi^3 + \frac{1}{3}\xi^2 + \frac{1}{3}\xi$
4	$\frac{1}{4}\xi^4 + \frac{1}{4}\xi^3 + \frac{1}{4}\xi^2 + \frac{1}{4}\xi$
5	$\frac{1}{5}\xi^5 + \frac{1}{5}\xi^4 + \frac{1}{5}\xi^3 + \frac{1}{5}\xi^2 + \frac{1}{5}\xi$
non-poly.	$(\exp(4\xi) - 1)/(\exp(4) - 1)$

Grid functions for variable Jacobian

Functional error $|\mathcal{I}(\mathcal{U}) - \mathcal{I}_h(\boldsymbol{u}_h)|$ convergence rate results

- LG operators converge at $\tau + 1$ only when grid function is a polynomial whose degree is less than or equal to the degree of the SBP operator used to approximate the Jacobian/ metrics

	ξ	$\frac{1}{2}\xi^2 + \frac{1}{2}\xi$	$\frac{1}{3}\xi^3 + \frac{1}{2}\xi^2 + \frac{1}{3}\xi$	$\frac{1}{4}\xi^4 + \frac{1}{4}\xi^3 + \frac{1}{4}\xi^2 + \frac{1}{4}\xi$	$\frac{1}{5}\xi^5 + \frac{1}{5}\xi^4 + \frac{1}{5}\xi^3 + \frac{1}{5}\xi^2 + \frac{1}{5}\xi$	$(\exp(4\xi) - 1)/(\exp(4) - 1)$
Operator	MFD1	MFD2	MFD3	MFD4	MFD5	MFNP
LGLp1	2.00	2.01	1.98	1.98	1.99	1.99
LGLp2	4.00	4.20	4.00	4.00	4.00	4.00
LGLp3	6.00	5.98	6.05	5.80	5.66	6.89
LGLp4	8.40	8.64	8.01	7.92	7.83	7.84
LGp1	4.01	**2.00**	**1.99**	**1.97**	**1.97**	**1.95**
LGp2	6.00	5.95	**2.00**	**2.00**	**2.00**	**2.00**
LGp3	8.69	7.96	8.23	**3.96**	**4.02**	**4.01**
LGp4	9.48	9.38	10.39	10.75	**4.00**	**4.01**

Representative functional error convergence rates for different grid functions. Cases that converge at less than $\tau + 1$ are **boxed**.

2D linear convection equation

Goal:

1. derive four dual-consistent discretizations of 2D linear convection equation based on mortar-element and global SBP-operator approaches*
2. characterize discretizations with respect to truncation error, solution accuracy, and functional accuracy

Linear convection equation and functional in physical space:

$$\sum_{m=1}^{2} \frac{\partial (a_m \mathcal{U})}{\partial x_m} = \mathcal{F} \quad \text{in } \Omega, \quad \mathcal{I}(\mathcal{U}) := \int_{\Omega} \mathcal{G}\mathcal{U}\, d\Omega + \oint_{\Gamma^+} \psi \boldsymbol{n} \cdot (\boldsymbol{a}\mathcal{U})\, d\Gamma$$

Discretize two analytically equivalent transformed PDEs:

$$\underbrace{\sum_{l,m=1}^{2} \frac{\partial}{\partial \xi_l} \left(\mathcal{J} \frac{\partial \xi_l}{\partial x_m} \mathcal{U} \right) = \mathcal{J}\mathcal{F},}_{\text{divergence}} \quad \underbrace{\frac{1}{2} \sum_{l,m=1}^{2} \left\{ \frac{\partial}{\partial \xi_l} \left(\mathcal{J} \frac{\partial \xi_l}{\partial x_m} \mathcal{U} \right) + \mathcal{J} \frac{\partial \xi_l}{\partial x_m} \frac{\partial \mathcal{U}}{\partial \xi_l} \right\} = \mathcal{J}\mathcal{F}}_{\text{skew-symmetric}}$$

Volume metric invariants used to obtain transformed equations:

$$\sum_{l=1}^{2} \frac{\partial}{\partial \xi_l} \left(\mathcal{J} \frac{\partial \xi_l}{\partial x_m} \right) = 0, \quad m = 1, 2$$

* based on Del Rey Fernández *et al.* [JSC 2019]

Mortar-element discretization (divergence)

Discrete PDE (interior element):

$$\sum_{l,m=1}^{2} \mathsf{D}_{\xi_l} \operatorname{diag}\left(\mathcal{J}\frac{\partial \xi_l}{\partial x_m}\right)_h \boldsymbol{u}_h = \operatorname{diag}\left(\mathcal{J}_h\right)\boldsymbol{f} + \mathsf{H}^{-1}\sum_{l,m=1}^{2} \mathsf{E}_{\xi_l} \operatorname{diag}\left(\mathcal{J}\frac{\partial \xi_l}{\partial x_m}\right)_h \boldsymbol{u}_h$$

$$- \mathsf{H}^{-1}\sum_{l,m=1}^{2}\left\{-\frac{1}{2}\mathsf{R}^{\mathrm{T}}_{\alpha_{\xi_l}}\mathsf{H}^{\perp}_{\xi_l}\operatorname{diag}\left(\mathcal{J}\frac{\partial \xi_l}{\partial x_m}\right)_h^{[2l-1]}(\mathsf{R}_{\alpha_{\xi_l}}\boldsymbol{u}_h + \boldsymbol{u}_{[2l-1]})\right\}$$

$$+ \mathsf{H}^{-1}\sum_{l,m=1}^{2}\left\{-\frac{1}{2}\mathsf{R}^{\mathrm{T}}_{\beta_{\xi_l}}\mathsf{H}^{\perp}_{\xi_l}\operatorname{diag}\left(\mathcal{J}\frac{\partial \xi_l}{\partial x_m}\right)_h^{[2l]}(\mathsf{R}_{\beta_{\xi_l}}\boldsymbol{u}_h + \boldsymbol{u}_{[2l]})\right\}$$

Discrete functional (single element):

$$\mathcal{I}_h(\boldsymbol{u}_h) = \boldsymbol{g}^{\mathrm{T}}\mathsf{H}\operatorname{diag}\left(\mathcal{J}_h\right)\boldsymbol{u}_h$$

$$- \frac{1}{2}\sum_{l=1}^{2}\boldsymbol{\psi}^{\mathrm{T}}_{[2l-1]}\mathsf{H}^{\perp}_{\xi_l}\left(\sum_{m=1}^{2}\operatorname{diag}\left(\mathcal{J}\frac{\partial \xi_l}{\partial x_m}\right)_h^{[2l-1]} - \left|\sum_{m=1}^{2}\operatorname{diag}\left(\mathcal{J}\frac{\partial \xi_l}{\partial x_m}\right)_h^{[2l-1]}\right|\right)\mathsf{R}_{\alpha_{\xi_l}}\boldsymbol{u}_h$$

$$+ \frac{1}{2}\sum_{l=1}^{2}\boldsymbol{\psi}^{\mathrm{T}}_{[2l]}\mathsf{H}^{\perp}_{\xi_l}\left(\sum_{m=1}^{2}\operatorname{diag}\left(\mathcal{J}\frac{\partial \xi_l}{\partial x_m}\right)_h^{[2l]} + \left|\sum_{m=1}^{2}\operatorname{diag}\left(\mathcal{J}\frac{\partial \xi_l}{\partial x_m}\right)_h^{[2l]}\right|\right)\mathsf{R}_{\beta_{\xi_l}}\boldsymbol{u}_h$$

Global SBP-operator discretization (skew-symmetric)

Discrete PDE (interior element):

$$\frac{1}{2}\sum_{l,m=1}^{2}\left\{\mathsf{D}_{\xi_l}\,\mathrm{diag}\left(\mathcal{J}\frac{\partial \xi_l}{\partial x_m}\right)_h + \mathrm{diag}\left(\mathcal{J}\frac{\partial \xi_l}{\partial x_m}\right)_h \mathsf{D}_{\xi_l}\right\}\boldsymbol{u}_h = \mathrm{diag}\left(\mathcal{J}_h\right)\boldsymbol{f}$$

$$+\,\mathsf{H}^{-1}\frac{1}{4}\sum_{l,m=1}^{2}\left\{\mathsf{E}_{\xi_l}\,\mathrm{diag}\left(\mathcal{J}\frac{\partial \xi_l}{\partial x_m}\right)_h + \mathrm{diag}\left(\mathcal{J}\frac{\partial \xi_l}{\partial x_m}\right)_h \mathsf{E}_{\xi_l}\right\}\boldsymbol{u}_h$$

$$-\,\frac{1}{4}\mathsf{H}^{-1}\sum_{l,m=1}^{2}\left\{\mathsf{R}^{\mathrm{T}}_{\beta\xi_l}\,\mathsf{H}^{\perp}_{\xi_l}\mathsf{R}_{\alpha\xi_l}\,\mathrm{diag}\left(\mathcal{J}\frac{\partial \xi_l}{\partial x_m}\right)_h^{(2l)}\boldsymbol{u}_{(2l)} - \mathsf{R}^{\mathrm{T}}_{\alpha\xi_l}\,\mathsf{H}^{\perp}_{\xi_l}\mathsf{R}_{\beta\xi_l}\,\mathrm{diag}\left(\mathcal{J}\frac{\partial \xi_l}{\partial x_m}\right)_h^{(2l-1)}\boldsymbol{u}_{(2l-1)}\right\}$$

$$-\,\frac{1}{4}\mathsf{H}^{-1}\sum_{l,m=1}^{2}\left\{\mathrm{diag}\left(\mathcal{J}\frac{\partial \xi_l}{\partial x_m}\right)_h \mathsf{R}^{\mathrm{T}}_{\beta\xi_l}\,\mathsf{H}^{\perp}_{\xi_l}\mathsf{R}_{\alpha\xi_l}\,\boldsymbol{u}_{(2l)} - \mathrm{diag}\left(\mathcal{J}\frac{\partial \xi_l}{\partial x_m}\right)_h \mathsf{R}^{\mathrm{T}}_{\alpha\xi_l}\,\mathsf{H}^{\perp}_{\xi_l}\mathsf{R}_{\beta\xi_l}\,\boldsymbol{u}_{(2l-1)}\right\}$$

Single-element global SBP-operator discretization (skew-symmetric)

Discrete functional (single element):

$$
\begin{aligned}
\mathcal{I}_h(\boldsymbol{u}_h) &= \boldsymbol{g}^{\mathrm{T}} \mathsf{H}\, \mathrm{diag}\left(\mathcal{J}_h\right) \boldsymbol{u}_h \\
&- \frac{1}{2}\left\{ \frac{1}{2}\sum_{l=1}^{2} \left(\tilde{\mathsf{I}}_{\xi_l} \boldsymbol{\psi}_{[2l-1]}\right)^{\mathrm{T}} \mathsf{R}_{\alpha\xi_l}^{\mathrm{T}} \mathsf{H}_{\xi_l}^{\perp} \mathsf{R}_{\alpha\xi_l} \left(\sum_{m=1}^{2} \mathrm{diag}\left(\mathcal{J}\frac{\partial \xi_l}{\partial x_m}\right)_h - \left| \sum_{m=1}^{2} \mathrm{diag}\left(\mathcal{J}\frac{\partial \xi_l}{\partial x_m}\right)_h \right| \right) \boldsymbol{u}_h \right. \\
&+ \left. \frac{1}{2}\sum_{l=1}^{2} \left(\left(\sum_{m=1}^{2} \mathrm{diag}\left(\mathcal{J}\frac{\partial \xi_l}{\partial x_m}\right)_h - \left| \sum_{m=1}^{2} \mathrm{diag}\left(\mathcal{J}\frac{\partial \xi_l}{\partial x_m}\right)_h \right| \right) \tilde{\mathsf{I}}_{\xi_l} \boldsymbol{\psi}_{[2l-1]} \right)^{\mathrm{T}} \mathsf{R}_{\alpha\xi_l}^{\mathrm{T}} \mathsf{H}_{\xi_l}^{\perp} \mathsf{R}_{\alpha\xi_l} \boldsymbol{u}_h \right\} \\
&+ \frac{1}{2}\left\{ \frac{1}{2}\sum_{l=1}^{2} \left(\tilde{\mathsf{I}}_{\xi_l} \boldsymbol{\psi}_{[2l]}\right)^{\mathrm{T}} \mathsf{R}_{\beta\xi_l}^{\mathrm{T}} \mathsf{H}_{\xi_l}^{\perp} \mathsf{R}_{\beta\xi_l} \left(\sum_{m=1}^{2} \mathrm{diag}\left(\mathcal{J}\frac{\partial \xi_l}{\partial x_m}\right)_h + \left| \sum_{m=1}^{2} \mathrm{diag}\left(\mathcal{J}\frac{\partial \xi_l}{\partial x_m}\right)_h \right| \right) \boldsymbol{u}_h \right. \\
&+ \left. \frac{1}{2}\sum_{l=1}^{2} \left(\left(\sum_{m=1}^{2} \mathrm{diag}\left(\mathcal{J}\frac{\partial \xi_l}{\partial x_m}\right)_h + \left| \sum_{m=1}^{2} \mathrm{diag}\left(\mathcal{J}\frac{\partial \xi_l}{\partial x_m}\right)_h \right| \right) \tilde{\mathsf{I}}_{\xi_l} \boldsymbol{\psi}_{[2l]} \right)^{\mathrm{T}} \mathsf{R}_{\beta\xi_l}^{\mathrm{T}} \mathsf{H}_{\xi_l}^{\perp} \mathsf{R}_{\beta\xi_l} \boldsymbol{u}_h \right\}
\end{aligned}
$$

Approximations of the metrics—mortar-element metrics

- baseline approach: approximate volume metrics on each element using standard approach (e.g., Thomas & Lombard [AIAA 1979]), approximate surface metrics by extrapolating volume metrics
- modified approach: use analytic surface metrics from mapping, use optimization technique of Crean *et al.* [JCP 2018] to approximate volume metrics

Discrete volume metric invariants (substitute constant solution):

$$\sum_{l=1}^{2} \frac{\partial}{\partial \xi_l} \left(\mathcal{J} \frac{\partial \xi_l}{\partial x_m} \right) = 0 = \sum_{l=1}^{2} \mathsf{D}_{\xi_l} \operatorname{diag} \left(\mathcal{J} \frac{\partial \xi_l}{\partial x_m} \right)_h \mathbf{1} - \mathsf{H}^{-1} \sum_{l=1}^{2} \left\{ \mathsf{E}_{\xi_l} \operatorname{diag} \left(\mathcal{J} \frac{\partial \xi_l}{\partial x_m} \right)_h \mathbf{1} \right.$$
$$\left. - \left(-\mathsf{R}^{\mathrm{T}}_{\alpha_{\xi_l}} \mathsf{H}^{\perp}_{\xi_l} \operatorname{diag} \left(\mathcal{J} \frac{\partial \xi_l}{\partial x_m} \right)^{[2l-1]}_h \mathbf{1}_{[2l-1]} + \mathsf{R}^{\mathrm{T}}_{\beta_{\xi_l}} \mathsf{H}^{\perp}_{\xi_l} \operatorname{diag} \left(\mathcal{J} \frac{\partial \xi_l}{\partial x_m} \right)^{[2l]}_h \mathbf{1}_{[2l]} \right) \right\}, \quad m = 1, 2$$

Discrete surface metric invariants (integrate volume metrics over domain):

$$\oint_{\hat{\Gamma}} \sum_{l=1}^{2} \left(\mathcal{J} \frac{\partial \xi_l}{\partial x_m} \right) n_{\xi_l} \, d\hat{\Gamma} = 0 =$$
$$\sum_{l=1}^{2} \mathbf{1}^{\mathrm{T}} \left(-\mathsf{R}^{\mathrm{T}}_{\alpha_{\xi_l}} \mathsf{H}^{\perp}_{\xi_l} \operatorname{diag} \left(\mathcal{J} \frac{\partial \xi_l}{\partial x_m} \right)^{[2l-1]}_h \mathbf{1}_{[2l-1]} + \mathsf{R}^{\mathrm{T}}_{\beta_{\xi_l}} \mathsf{H}^{\perp}_{\xi_l} \operatorname{diag} \left(\mathcal{J} \frac{\partial \xi_l}{\partial x_m} \right)^{[2l]}_h \mathbf{1}_{[2l]} \right), \quad m = 1, 2$$

Mortar-element metrics—modified approach*

Motivation:

- in 2D, for $p_g > p$, using the volume and surface metrics from the mapping does not satisfy the volume metric invariants

Modified approach: for $\mathrm{diag}\left(\mathcal{J}\frac{\partial \xi_1}{\partial x_1}\right)_h$ and $\mathrm{diag}\left(\mathcal{J}\frac{\partial \xi_2}{\partial x_1}\right)_h$, for example, solve the following local optimization problem on each element

$$\min_{\boldsymbol{m}} \frac{1}{2}(\boldsymbol{m}-\boldsymbol{m}_{\mathrm{target}})^{\mathrm{T}}(\boldsymbol{m}-\boldsymbol{m}_{\mathrm{target}}), \quad \text{subject to} \quad \mathsf{Q}^{\mathrm{T}}\boldsymbol{m}=\boldsymbol{c}$$

where

$$\mathsf{Q}^{\mathrm{T}} := \left[\mathsf{Q}_{\xi_1}^{\mathrm{T}}, \mathsf{Q}_{\xi_2}^{\mathrm{T}}\right],$$

$$\boldsymbol{m}^{\mathrm{T}} := \mathbf{1}^{\mathrm{T}}\left[\mathrm{diag}\left(\mathcal{J}\frac{\partial \xi_1}{\partial x_1}\right)_h, \mathrm{diag}\left(\mathcal{J}\frac{\partial \xi_2}{\partial x_1}\right)_h\right], \quad \text{and}$$

$$\boldsymbol{c} := \sum_{l=1}^{2} \mathbf{1}^{\mathrm{T}}\left(-\mathsf{R}_{\alpha\xi_l}^{\mathrm{T}}\mathsf{H}_{\xi_l}^{\perp}\,\mathrm{diag}\left(\mathcal{J}\frac{\partial \xi_l}{\partial x_1}\right)^{[2l-1]}\mathbf{1}_{[2l-1]} + \mathsf{R}_{\beta\xi_l}^{\mathrm{T}}\mathsf{H}_{\xi_l}^{\perp}\,\mathrm{diag}\left(\mathcal{J}\frac{\partial \xi_l}{\partial x_1}\right)^{[2l]}\mathbf{1}_{[2l]}\right)$$

Solution to the local optimization problem:

$$\boldsymbol{m} = \boldsymbol{m}_{\mathrm{target}} - \left(\mathsf{Q}^{\mathrm{T}}\right)^{\dagger}\left(\mathsf{Q}^{\mathrm{T}}\boldsymbol{m}_{\mathrm{target}} - \boldsymbol{c}\right)$$

*see Crean *et al.* [JCP 2018] and Del Rey Fernández *et al.* [JSC 2019]

Approximations of the metrics—global SBP-operator metrics*

- global approach: use global SBP operators to approximate volume metric terms using standard approach

In 2D: process is straightforward

$$\operatorname{diag}\left(\mathcal{J}\frac{\partial \xi_1}{\partial x_1}\right)_h^g \mathbf{1}_g = \mathsf{D}_{\xi_2}^g \boldsymbol{x}_2^g, \qquad \operatorname{diag}\left(\mathcal{J}\frac{\partial \xi_1}{\partial x_2}\right)_h^g \mathbf{1}_g = -\mathsf{D}_{\xi_2}^g \boldsymbol{x}_1^g$$

$$\operatorname{diag}\left(\mathcal{J}\frac{\partial \xi_2}{\partial x_1}\right)_h^g \mathbf{1}_g = -\mathsf{D}_{\xi_1}^g \boldsymbol{x}_2^g, \qquad \operatorname{diag}\left(\mathcal{J}\frac{\partial \xi_2}{\partial x_2}\right)_h^g \mathbf{1}_g = \mathsf{D}_{\xi_1}^g \boldsymbol{x}_1^g$$

In 3D: several options, e.g., Thomas & Lombard [AIAA 1979] (shown below), Deng *et al.* [JCP 2013], Vinokur & Yee [Front. of CFD 2001]

$$\operatorname{diag}\left(\mathcal{J}\frac{\partial \xi_1}{\partial x_1}\right)_h^g \mathbf{1}_g = \mathsf{D}_{\xi_3}^g \left(\operatorname{diag}(\boldsymbol{x}_3^g)\,\mathsf{D}_{\xi_2}^g \boldsymbol{x}_2^g\right) - \mathsf{D}_{\xi_2}^g \left(\operatorname{diag}(\boldsymbol{x}_3^g)\,\mathsf{D}_{\xi_3}^g \boldsymbol{x}_2^g\right)$$

$$\operatorname{diag}\left(\mathcal{J}\frac{\partial \xi_1}{\partial x_2}\right)_h^g \mathbf{1}_g = \mathsf{D}_{\xi_3}^g \left(\operatorname{diag}(\boldsymbol{x}_1^g)\,\mathsf{D}_{\xi_2}^g \boldsymbol{x}_3^g\right) - \mathsf{D}_{\xi_2}^g \left(\operatorname{diag}(\boldsymbol{x}_1^g)\,\mathsf{D}_{\xi_3}^g \boldsymbol{x}_3^g\right)$$

$$\operatorname{diag}\left(\mathcal{J}\frac{\partial \xi_1}{\partial x_3}\right)_h^g \mathbf{1}_g = \mathsf{D}_{\xi_3}^g \left(\operatorname{diag}(\boldsymbol{x}_2^g)\,\mathsf{D}_{\xi_2}^g \boldsymbol{x}_1^g\right) - \mathsf{D}_{\xi_2}^g \left(\operatorname{diag}(\boldsymbol{x}_2^g)\,\mathsf{D}_{\xi_3}^g \boldsymbol{x}_1^g\right)$$

$$\vdots$$

*see Del Rey Fernández *et al.* [JSC 2019]

2D scalar linear boundary-value problem

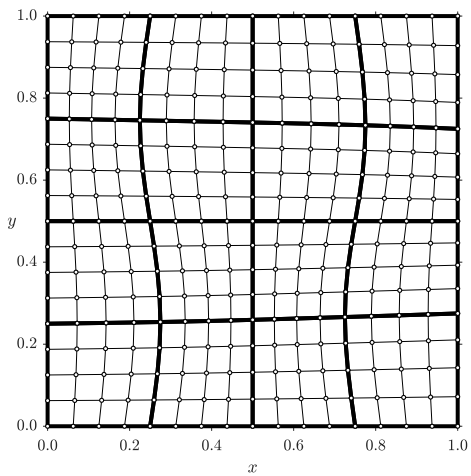
Purpose:

1. investigate impact of superparametric mapping
2. evaluate baseline, modified, and global approaches for the metrics in the context of the mortar-element and global SBP-operator approaches

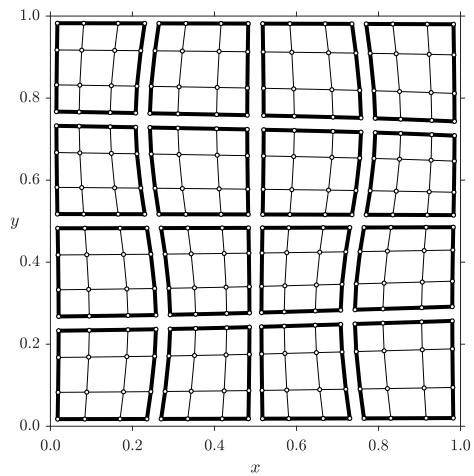
Problem parameters: primal and dual source terms defined such that

$$\mathcal{U}_{\text{exact}}(x, y) := \sin(2\pi x) + \sin(2\pi y) \text{ and}$$

$$\psi_{\text{exact}}(x, y) := \sin(2\pi x) + \frac{\exp(y) - 1}{\exp(1) - 1}$$



Initial grid with 5×5 uniform nodes in each element.



Final grid with 4×4 $p = 3$ LG nodes in each element.

Example high-order grid for Ω. A degree $p_g = 4$ element-local Lagrange mapping is defined on each element of the initial grid based on the uniform nodes.

Accuracy measures and test case matrix for 2D boundary-value problem

Accuracy measure	**Definition**
Primal truncation error	$\left\| \mathsf{J}_g^{-1}\mathsf{H}_g^{-1}(\mathsf{A}_g\boldsymbol{u}_g - \mathcal{F}_g) \right\|_\infty = \max \left\| \mathsf{J}_g^{-1}\mathsf{H}_g^{-1}(\mathsf{A}_g\boldsymbol{u}_g - \mathcal{F}_g) \right\|$
Primal solution error	$\left\| \boldsymbol{u}_{h,g} - \boldsymbol{u}_g \right\|_{\mathsf{H}_g} = \sqrt{(\boldsymbol{u}_{h,g} - \boldsymbol{u}_g)^{\mathrm{T}}\mathsf{H}_g(\boldsymbol{u}_{h,g} - \boldsymbol{u}_g)}$
Primal functional error	$\left\| \mathcal{I}_h(\boldsymbol{u}_{h,g}) - \mathcal{I}(\mathcal{U}) \right\|$
Dual truncation error	$\left\| \mathsf{J}_g^{-1}\mathsf{H}_g^{-1}(\mathsf{A}_g^{\mathrm{T}}\boldsymbol{\psi}_g - \mathcal{F}_g^{\mathsf{dual}}) \right\|_\infty = \max \left\| \mathsf{J}_g^{-1}\mathsf{H}_g^{-1}(\mathsf{A}_g^{\mathrm{T}}\boldsymbol{\psi}_g - \mathcal{F}_g^{\mathsf{dual}}) \right\|$
Dual solution error	$\left\| \boldsymbol{\psi}_{h,g} - \boldsymbol{\psi}_g \right\|_{\mathsf{H}_g} = \sqrt{(\boldsymbol{\psi}_{h,g} - \boldsymbol{\psi}_g)^{\mathrm{T}}\mathsf{H}_g(\boldsymbol{\psi}_{h,g} - \boldsymbol{\psi}_g)}$
Dual functional error	$\left\| \mathcal{I}_h(\boldsymbol{\psi}_{h,g}) - \mathcal{I}(\psi) \right\|$

Accuracy measures

Type of discretization	**Form of equation**	**Metrics**	**Mapping**	p_g
Mortar-element	Div/Skew	Baseline	Lagrange	p
Mortar-element	Div/Skew	Baseline	Lagrange	$p+1$
Mortar-element	Div/Skew	Modified	Lagrange	$p+1$
Global SBP-operator	Div/Skew	Global	Lagrange	p
Global SBP-operator	Div/Skew	Global	Lagrange	$p+1$

Test case matrix

Summary of results for 2D boundary-value problem

- skew-symmetric and divergence accuracy results similar
- all truncation error rates approximately p, all solution error rates approximately $p+1$ with LG generally outperforming LGL
- best-case LG functional convergence rate of $2p+1$ outperforms best-case LGL functional convergence rate of $2p$ (in the tables below, ✔-marks indicate functional superconvergence, ✘-marks indicate no superconvergence)

Operator	**Baseline,** p	**Baseline,** $p+1$	**Modified,** $p+1$
LGL	✔	✔	✔
LG	✔	✘	✔

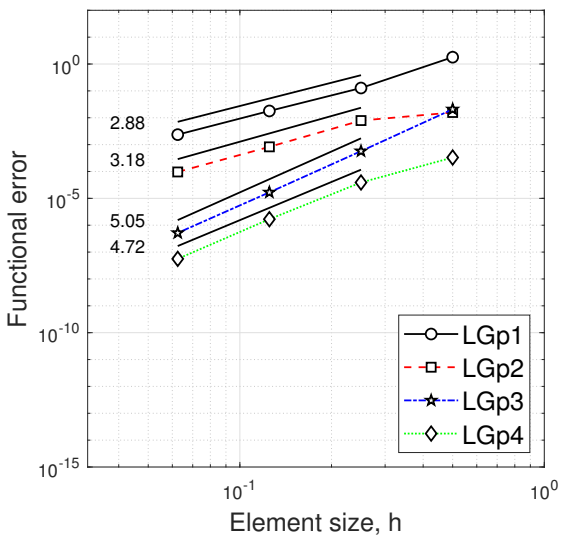
Mortar-element approach superconvergence matrix (metrics $=$ baseline or modified, degree of mapping $=p$ or $p+1$)

Operator	**Global,** p	**Global,** $p+1$
LGL	✔	✔
LG	✔	✘

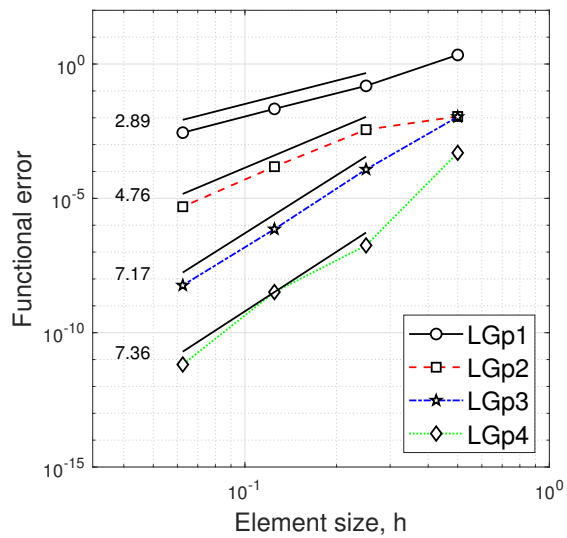
Global SBP-operator approach superconvergence matrix (metrics $=$ global, degree of mapping $=p$ or $p+1$)

Conclusions (linear convection equation)

- in Del Rey Fernández *et al.* [JSC 2019], lack of conservation with LG discretizations with baseline metrics in 3D highlighted as motivating factor for using modified metrics, here it is concluded that consideration of functional accuracy provides strong motivation for modified metrics for LG
- functional accuracy identified as a criterion for potentially preferring the mortar-element approach over the global SBP-operator approach, due to the ability of the mortar-element approach to obtain superconvergence with LG operators in 2D with $p+1$ mappings when using modified metrics



LG, $p+1$, global.



LG, $p+1$, modified.

Comparison of skew-symmetric discretizations of the linear convection equation. Global SBP-operator approach on left, mortar-element approach on right.

Accurate solutions and functionals for the Euler equations

Goal:

- derive dual-consistent mortar-element discretization of Euler equations that leads to accurate solutions and functionals

Boundary force functional:

$$\mathcal{I}(\boldsymbol{\mathcal{U}}) := \int_{\hat{\Gamma}} i(\boldsymbol{\mathcal{U}})\, d\hat{\Gamma} = \int_{\hat{\Gamma}_{\mathrm{W}}} \breve{\boldsymbol{\phi}}^{\mathrm{T}} \left\{ \boldsymbol{n} \cdot \boldsymbol{\mathcal{F}}(\mathsf{P}\boldsymbol{\mathcal{U}}) \right\} d\hat{\Gamma}$$

where $i(\boldsymbol{\mathcal{U}}) := \breve{\boldsymbol{\phi}}^{\mathrm{T}} \left\{ \boldsymbol{n} \cdot \boldsymbol{\mathcal{F}}(\mathsf{P}\boldsymbol{\mathcal{U}}) \right\}$ on $\hat{\Gamma}_{\mathrm{W}}$ and $i(\boldsymbol{\mathcal{U}}) := 0$ on $\hat{\Gamma} \setminus \hat{\Gamma}_{\mathrm{W}}$*

Discrete Euler equations (single element):

$$\sum_{l,m=1}^{2} \mathsf{D}_{\xi_l} \operatorname{diag}\left(\widetilde{\mathcal{J} \frac{\partial \xi_l}{\partial x_m}} \right)_h \boldsymbol{f}_{x_m}(\boldsymbol{u}_h) = \mathrm{SAT}^{\boldsymbol{u}_h}_{(2l-1)} + \mathrm{SAT}^{\boldsymbol{u}_h}_{(2l)}$$

where, for example,

$$\mathrm{SAT}^{\boldsymbol{u}_h}_{(2l-1)} := \mathsf{H}^{-1} \sum_{l=1}^{2} \left\{ -\mathsf{R}^{\mathrm{T}}_{\alpha_{\xi_l}} \mathsf{H}^{\perp}_{\xi_l} \left(\boldsymbol{f}_{(2l-1),h}(\boldsymbol{u}_h) - \boldsymbol{f}^{\star}_{(2l-1),h}(\boldsymbol{u}_h) \right) \right\}$$

*see Hicken & Zingg [JCP 2014] and Hartmann & Leicht [JCP 2015] for details

Accuracy of the flow tangency boundary condition

Background:

- several papers (e.g., Bassi & Rebay [JCP 1997], Zwanenburg & Nadarajah [AIAA 2017]) demonstrate that superparametric geometry representations provide an accuracy benefit with respect to solution error in the presence of flow tangency boundary conditions

Wall SAT:

$$\mathrm{SAT}^{\boldsymbol{u}}_{\mathrm{Wall}} := -\mathsf{H}^{-1}\mathsf{R}^{\mathrm{T}}_{\alpha_{\xi_2}}\mathsf{H}^{\perp}_{\xi_2}\sum_{m=1}^{2}\left\{\mathsf{R}_{\alpha_{\xi_2}}\,\mathrm{diag}\left(\widetilde{\mathcal{J}\frac{\partial \xi_2}{\partial x_m}}\right)_h \boldsymbol{f}_{x_m}(\boldsymbol{u}) - \mathrm{diag}\left(\widetilde{\mathcal{J}\frac{\partial \xi_2}{\partial x_m}}\right)^{[3]}_h \boldsymbol{f}_{x_m}(\tilde{\mathsf{P}}_h\mathsf{R}_{\alpha_{\xi_2}}\boldsymbol{u})\right\}$$

Consistency condition:

$$\left\|\mathrm{diag}\left(\mathcal{J}_h\right)^{-1}\mathrm{SAT}^{\boldsymbol{u}}_{\mathrm{Wall}}\right\|_{\infty} = \mathcal{O}(h^p)$$

Theorem

Assuming that a degree p_g polynomial geometry representation is used in each element and assuming that the wall normals are constructed directly from the degree p_g geometry representation, the wall boundary SAT satisfies the consistency condition if and only if $p_g \geq p+1$, where p_g and p are integers.

Result:

$$\left\|\mathrm{diag}\left(\mathcal{J}_h\right)^{-1}\mathrm{SAT}^{\boldsymbol{u}}_{\mathrm{Wall}}\right\|_{\infty} = \mathcal{O}(h^r) + \mathcal{O}(h^{p_g-1})$$

Unsteady isentropic vortex—exact solution to the Euler equations*

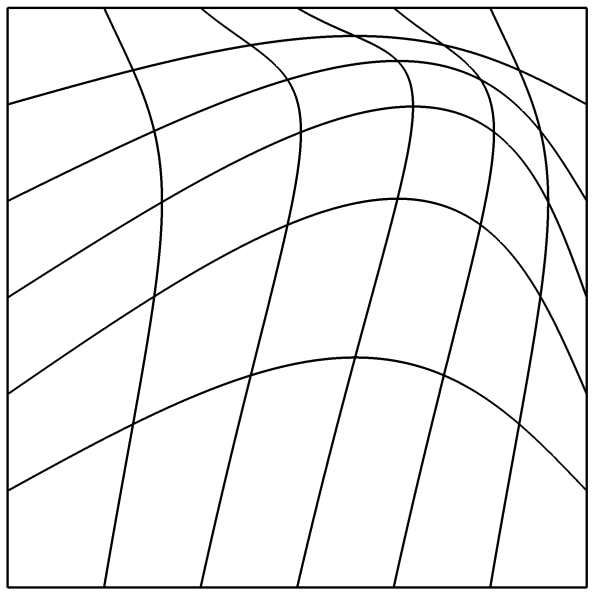
Purpose:

1. verify accuracy of novel volume dissipation models for use with hybrid Gauss-trapezoidal-Lobatto (HGTL) and Mattsson *et al.*'s optimal "Accurate" (MattAcc) operators

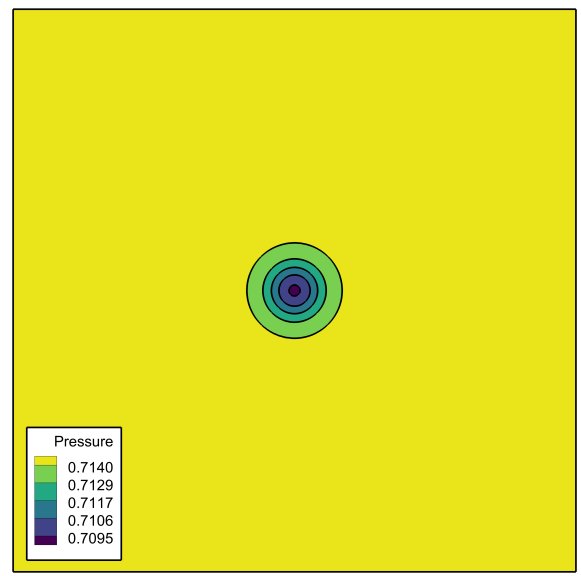
$$\mathsf{A}_\mathsf{D} = -\varepsilon \Delta x_{\text{avg}}^{2s-1} \mathsf{H}^{-1} \mathsf{M}^{\mathrm{T}} \mathsf{C} \mathsf{M}$$

2. investigate effect of different values of volume dissipation coefficient ε on accuracy

Problem parameters: $M_\infty = 0.5$, $[x, y] \in [-5, 5]^2$, RK4 time-marching



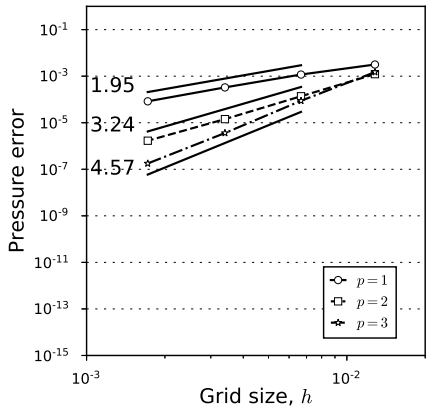
Grid with 36 elements (only element boundaries shown)



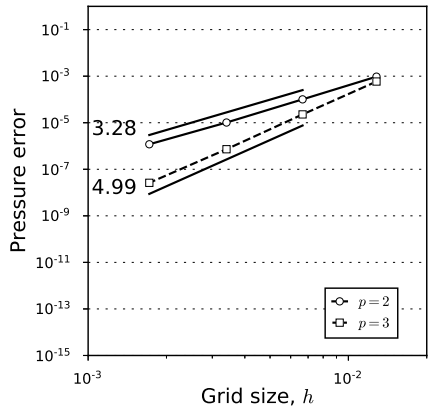
Numerical pressure contours with degree $p = 3$ CSBP operators at time $t = 20$

*see Wang *et al.* [Int. J. Numer. Methods Fluids 2013] and Spiegel *et al.* [AIAA 2015]

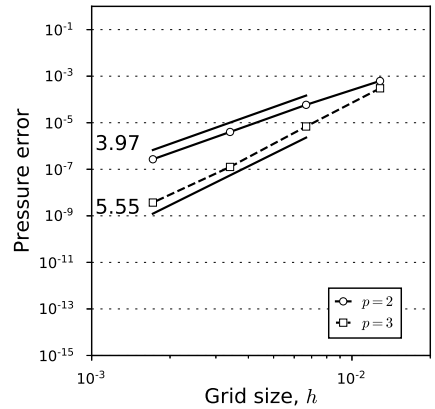
Unsteady isentropic vortex



CSBP, $\varepsilon = 0$.

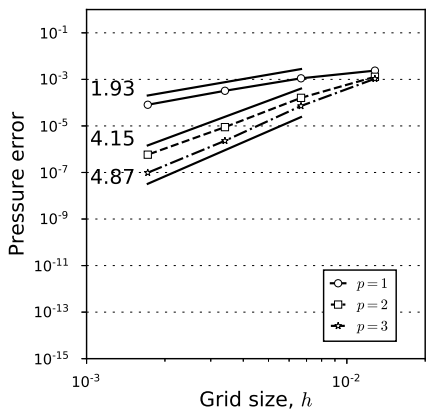


HGTL, $\varepsilon = 0$.

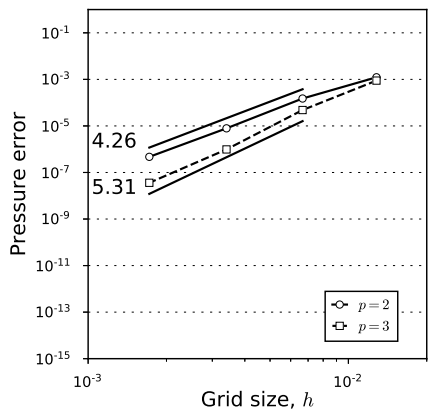


MattAcc, $\varepsilon = 0$.

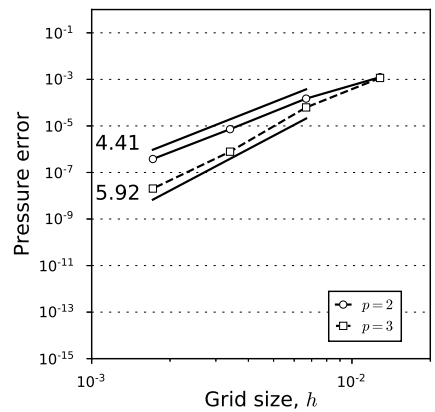
When $\varepsilon = 0$: MattAccp3 has nearly 10^2 benefit in terms of pressure error accuracy over CSBPp3



CSBP, $\varepsilon = 0.025$.



HGTL, $\varepsilon = 0.025$.



MattAcc, $\varepsilon = 0.025$.

When $\varepsilon = 0.025$: MattAccp3 has under 10^1 benefit in terms of pressure error accuracy over CSBPp3

Convergence of pressure error for the unsteady isentropic vortex problem governed by the Euler equations. The caption of each sub plot indicates the operator and volume dissipation coefficient ε, respectively. Note that $\varepsilon = 0$ means that no volume dissipation is used.

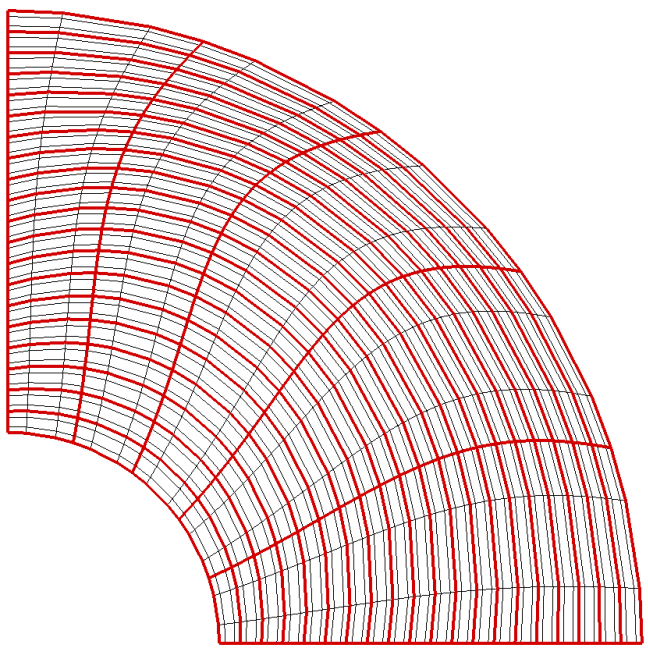
Steady isentropic vortex—exact solution to the Euler equations*

Purpose:

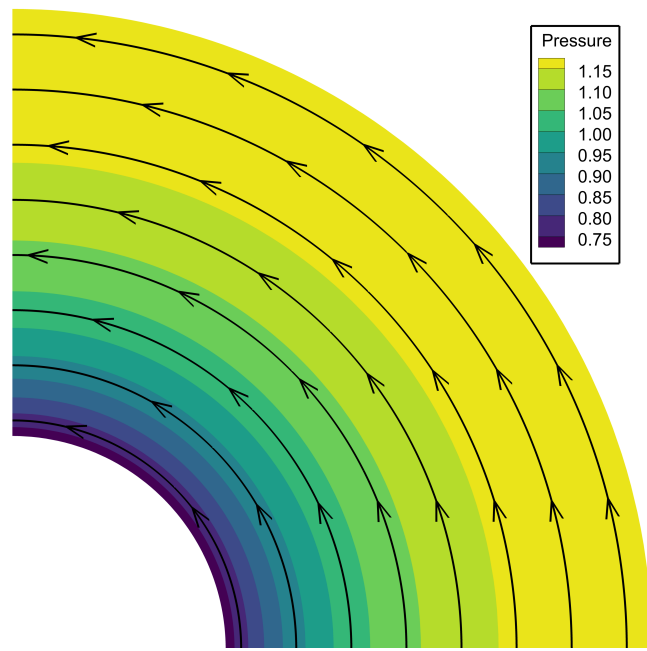
1. investigate impact of superparametric mapping on LGL/ LG schemes
2. characterize and compare baseline and modified approaches for the metrics
3. compare Lagrange and B-spline approaches for high-order grids
4. investigate impact of wall normal accuracy on traditional schemes
5. functional accuracy of traditional operators with element-type refinement

Problem parameters:

- $M_{\text{in}} = 0.95$, $\rho_{\text{in}} = 2$, $\text{AR} \approx 3$ near inner radius $r_{\text{in}} = 1$
- Exact drag force functional $= -1/\gamma$, defined on inner radius



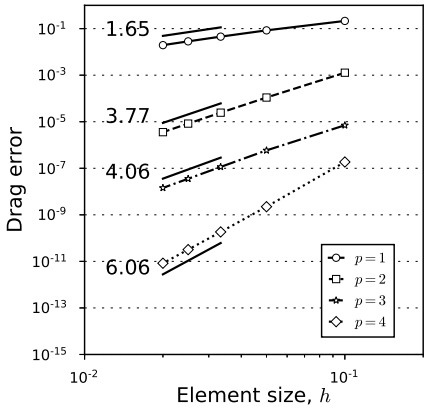
Degree $p = 3$ LGL nodes on coarsest grid



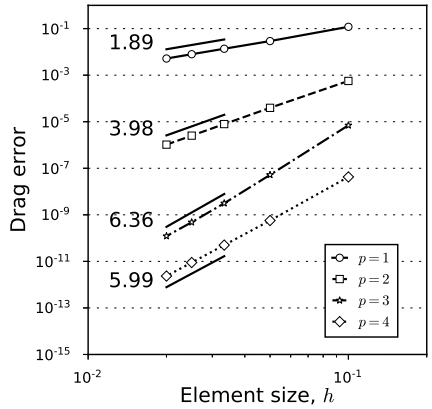
Pressure contours and velocity streamlines

*see Hicken & Zingg [SISC 2011, JCP 2014]

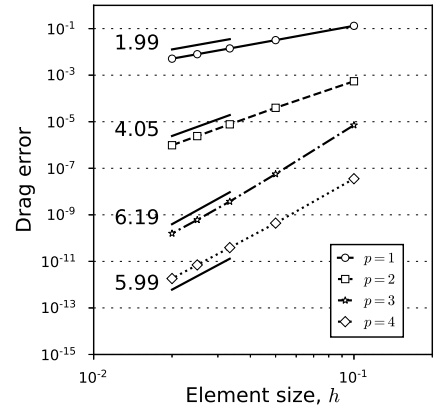
Effect of degree of mapping and approaches for metrics



LGL, p, baseline.

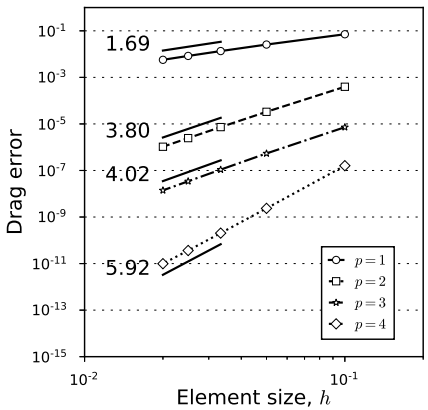


LGL, $p+1$, baseline.

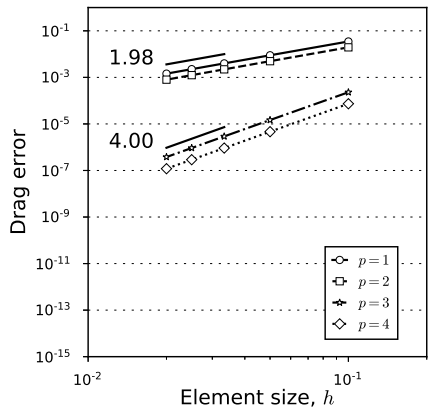


LGL, $p+1$, modified.

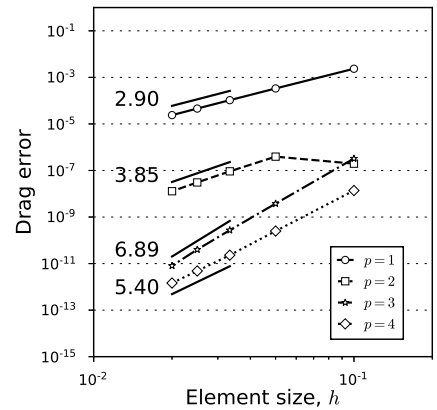
LGL superconverges with $p+1$, baseline or modified metrics



LG, p, baseline.



LG, $p+1$, baseline.

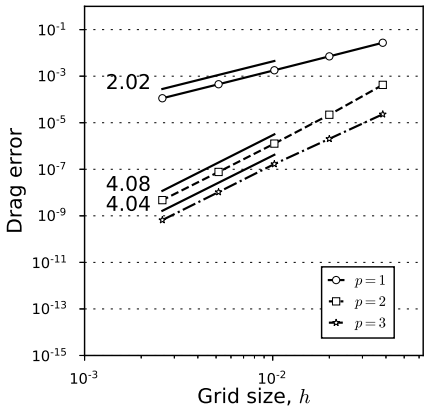


LG, $p+1$, modified.

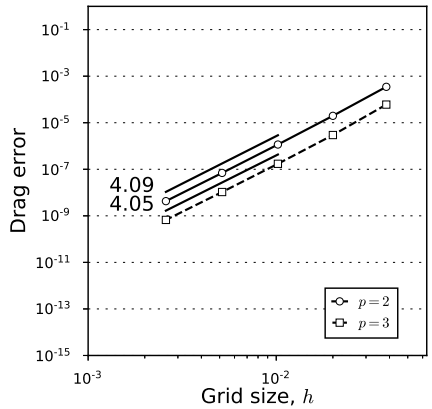
LG superconverges with $p+1$, modified metrics

Convergence of drag error for the steady isentropic vortex problem governed by the Euler equations. The caption of each sub plot indicates the operator, degree of mapping, and approach for the metrics, respectively. Lagrange mappings are used.

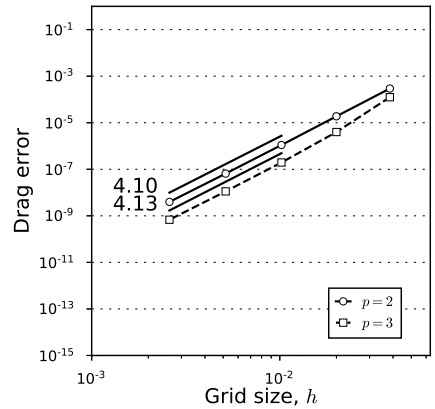
Effect of accuracy of normal with traditional refinement



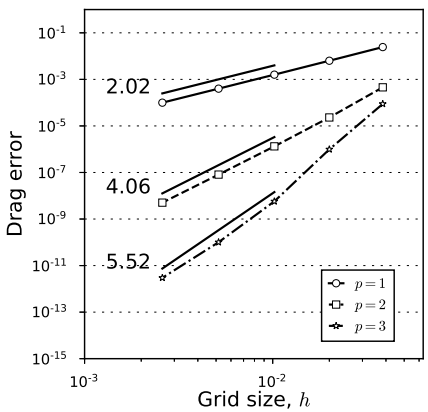
CSBP, p, baseline.



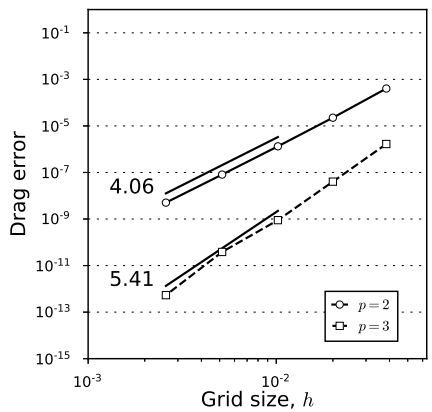
HGTL, p, baseline.



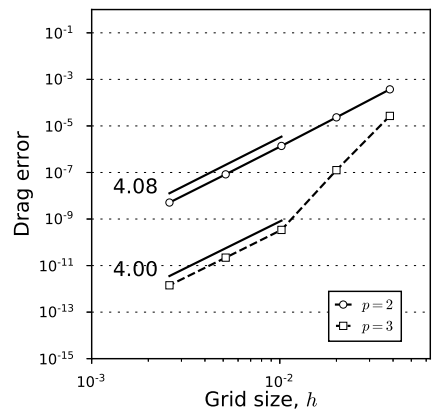
MattAcc, p, baseline.



CSBP, $p+1$, baseline.



HGTL, $p+1$, baseline.



MattAcc, $p+1$, baseline.

benefit of using $p+1$ one-sided stencils for normal noticeable for $p=3$ operators, not $p=1,2$ operators for this problem

Convergence of drag error for the steady isentropic vortex problem governed by the Euler equations. The caption of each sub plot indicates the operator, degree of normal, and approach for the metrics, respectively. Traditional refinement is used with the exact analytical mapping.

Subsonic channel flow over a Gaussian bump—Euler equations*

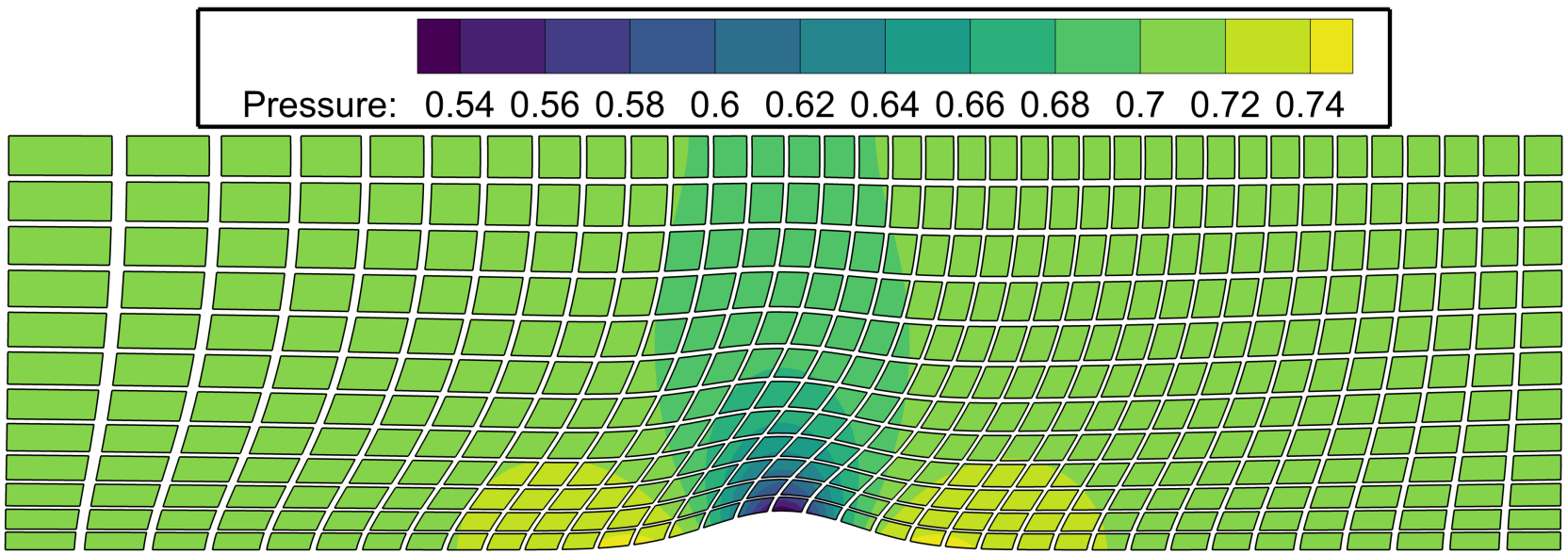
Purpose:

1. investigate degree of mapping and approaches for metrics
2. investigate efficiency with respect to total DOFs and core hours

Problem parameters: $M_\infty = 0.5$, inflow/ outflow and wall boundary conditions

- Weighted lift functional (approximated with LGp4 with modified metrics)

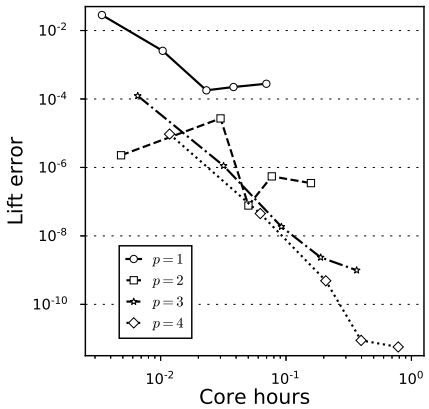
$$\mathcal{I}(\boldsymbol{u}) = \int_{x_1 \in [-1.5, 1.5],\, x_2 = \frac{3}{32} \mathrm{e}^{-25 x_1^2}} n_{x_2} p(\boldsymbol{u}) \mathrm{e}^{-8 x_1^2} \, ds$$



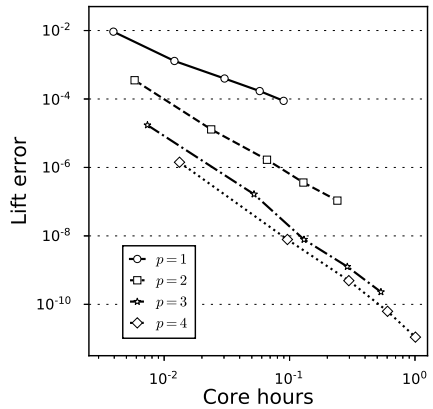
Numerical pressure contours and grid. Degree $p = 3$ Legendre-Gauss generalized summation-by-parts operators are used in each element (only element boundaries shown).

*see Lu [PhD thesis 2005] for a similar test problem

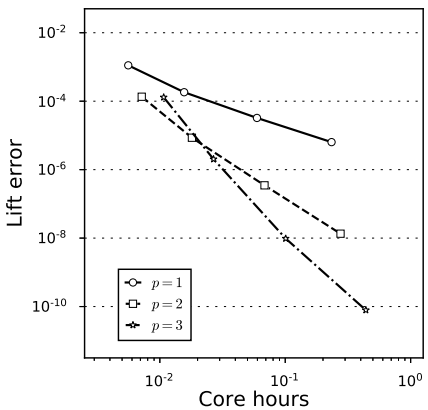
Efficiency with respect to core hours



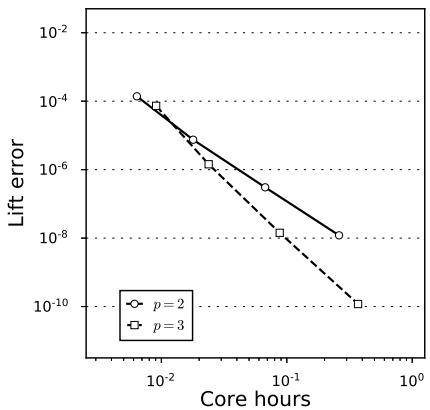
LGL, $p+1$, modified.



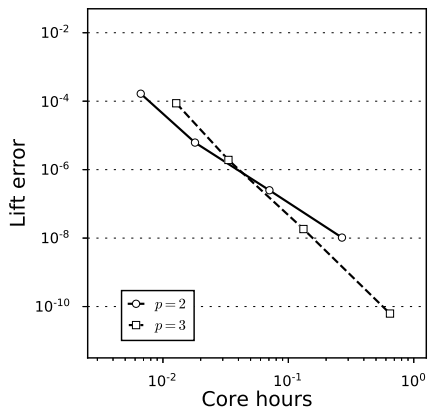
LG, $p+1$, modified.



CSBP, exact, baseline.



HGTL, exact, baseline.



MattAcc, exact, baseline.

traditional schemes can be more efficient w.r.t. core hours due to reduced number of SATs/ increased sparsity

Convergence of lift error as a function of core hours for the subsonic channel flow over a Gaussian bump problem governed by the Euler equations. The caption of each sub plot indicates the operator, degree of mapping, and approach for the metrics, respectively. Lagrange mappings are used for the LGL and LG schemes.

Conclusions (Euler equations)

- shown theoretically that degree of mapping related to accuracy of flow tangency boundary condition through accuracy of wall normal
- suboptimal functional convergence generally observed with degree p mappings/ degree p one-sided stencils, due to reduced accuracy of wall normal

Operator	**Baseline,** p	**Baseline,** $p+1$	**Modified,** $p+1$
LGL	✘ (wall normal)	✔	✔
LG	✘ (wall normal)	✘	✔

Mortar-element approach superconvergence matrix (metrics $=$ baseline or modified, degree of mapping $= p$ or $p+1$)

- optimal "Accurate" operators of Mattsson *et al.* (MattAcc) generally perform better than CSBP/ HGTL w.r.t. solution error, not much difference between different families of operators in terms of functional error
- benefit of MattAcc with respect to solution error reduced with addition of volume dissipation
- purely element-type operators generally more efficient w.r.t. total DOFs; however, traditional schemes can be more efficient w.r.t. core hours due to reduced number of SATs/ increased sparsity

Summary and future work

Main objectives:

1. Develop components of high-order flow solvers.
   - constructed volume dissipation operators based on HGTL, HGT, and Mattsson *et al.* nodes, characterized portion of operators through numerical studies
   - presented two procedures for high-order grid generation and refinement
2. Show that functional superconvergence is retained for generalized SBP discretizations of the linear convection equation in curvilinear coordinates.
   - presented and verified 1D functional accuracy estimate
   - derived and characterized four dual-consistent discretizations of 2D linear convection equation
3. Develop generalized SBP methods for obtaining superconvergent functionals when solving sufficiently smooth problems governed by the Euler equations.
   - derived and characterized dual-consistent discretization of 2D Euler equations
   - delineated conditions for superconvergence—mapping, metrics, wall normal

Future work:

- NS & RANS, discontinuities (geometric singularities), 3D problems, dense-norm operators, nonpolynomial mappings (NURBS), entropy stable schemes, unstructured grids

Financial and/ or computational support provided by:

NSERC CRSNG

Ontario

UNIVERSITY OF TORONTO

compute canada | calcul canada

SciNet
ADVANCED RESEARCH COMPUTING at the UNIVERSITY OF TORONTO